How to cite: *Angew. Chem. Int. Ed.* **2020**, *59*, 10327–10331
International Edition: doi.org/10.1002/anie.201916718
German Edition: doi.org/10.1002/ange.201916718

Fluorescent Probes

A Small-Molecule AIE Chromosome Periphery Probe for Cytogenetic Studies

*Ming-Yu Wu, Jong-Kai Leung, Li Liu, Chuen Kam, Kelvin Yuen Kwong Chan, Ronald A. Li, Shun Feng, and Sijie Chen**

Abstract: *The chromosome periphery (CP) is a complex network that covers the outer surface of chromosomes. It acts as a carrier of nucleolar components, helps maintain chromosome structure, and plays an important role in mitosis. Current methods for fluorescence imaging of CP largely rely on immunostaining. We herein report a small-molecule fluorescent probe,* ***ID-IQ****, which possesses aggregation-induced emission (AIE) property, for CP imaging. By labelling the CP,* ***ID-IQ*** *sharply highlighted the chromosome boundaries, which enabled rapid segmentation of touching and overlapping chromosomes, direct identification of the centromere, and clear visualization of chromosome morphology.* ***ID-IQ*** *staining was also compatible with fluorescence in situ hybridization and could assist the precise location of the gene in designated chromosome. Altogether, this study provides a versatile cytogenetic tool for improved chromosome analysis, which greatly benefits the clinical diagnostic testing and genomic research.*

Cytogenetic analysis, which focuses on the analysis of chromosomes and related abnormalities, is an important clinical diagnostic test widely used in oncology, haematology, perinatology, or obstetrics studies[1] as well as a standard cell characterization approach in quality control of induced pluripotent stem cells (iPSCs) for cell therapy.[2] The cytogenetic studies include the study of the chromosome number, structure and, gene locus in the chromosome. Karyotyping and fluorescence in situ hybridization (FISH) are two standard techniques in cytogenetics, which have had great success.[3] However, cytogeneticists often face challenges when attempting to separate touching or overlapping chromosomes, directly localize the centromere region, and find a clear landmark to map gene loci.[4] A tool that can visualize the chromosome boundary will help researchers to overcome these obstacles and greatly facilitate the cytogenetic analysis.

Though the first description of a sheath-like structure covering the surface of mitotic chromosomes was made more than a century ago,[5] the molecular nature of such complexes, named the chromosome periphery (CP), has been identified recently.[6] The CP is proposed to be an insulator or barrier to protect chromosomes from subcellular environment during cell division and is a carrier of nuclear and nucleolar components to equally distribute duplicated chromosomes to daughter cells.[7] However, it is one of the chromosomal compartments that is poorly understood.[8] Currently, techniques such as immunofluorescence or ectopically expressed genes fused with the fluorescent protein are extensively used to investigate some specific chromosome periphery proteins (CPPs) such as Ki-67, Ku70/80 complex, or Bcl2.[9] Nonetheless, immunolabelling of a specific CPP may overlook the whole structure of the CP and its overall functionality. Furthermore, there is not yet any reported small organic fluorescent dye for CP imaging. Thus, it is highly desirable to develop such a probe for both CP studies and cytogenetic studies.

Fluorescence imaging is an indispensable technique for visualizing biomolecules and structures, tracking physiological and pathological processes, and diagnosing diseases in complex biological systems.[10] Recently, fluorescent probes with aggregation-induced emission (AIE) property have emerged as a group of excellent candidates for bioimaging.[11] In contrast to conventional probes with self-quenching problems, AIE luminogens show weak or undetectable emission in dilute solution but emit strong fluorescence in the aggregated or solid state. Therefore, AIE probes usually enjoy low background fluorescence, strong signal-to-noise ratio, and good photostability.[12] AIE probes also exhibit superior turn-on fluorescence imaging for detection of cell organelles or biomacromolecules owing to the restriction of intramolecular motions of AIE fluorophores by the binding target.[13]

In this contribution, the first small-molecule fluorescent probe for CP imaging, **ID-IQ** (Figure 1), was developed. **ID-IQ** showed AIE property and could be widely used for imaging the CP in different cell types. With the use of **ID-IQ**,

[*] Dr. M.-Y. Wu, J.-K. Leung, Dr. C. Kam, Prof. Dr. R. A. Li, Dr. S. Chen
Ming Wai Lau Centre for Reparative Medicine, Karolinska Institutet
Hong Kong (China)
E-mail: sijie.chen@ki.se
Dr. M.-Y. Wu, L. Liu, Prof. Dr. S. Feng
School of Life Science and Engineering, Southwest Jiaotong University, Chengdu Sichuan 610031 (China)
Dr. K. Y. K. Chan
Department of Obstetrics and Gynaecology, Queen Mary Hospital
Hong Kong (China)
Dr. K. Y. K. Chan
Prenatal Diagnostic Laboratory, Tsan Yuk Hospital
Hong Kong (China)
Prof. Dr. R. A. Li, Dr. S. Chen
Dr. Li Dak-Sum Research Centre, The University of Hong Kong
Hong Kong (China)
Supporting information and the ORCID identification number(s) for the author(s) of this article can be found under: https://doi.org/10.1002/anie.201916718.

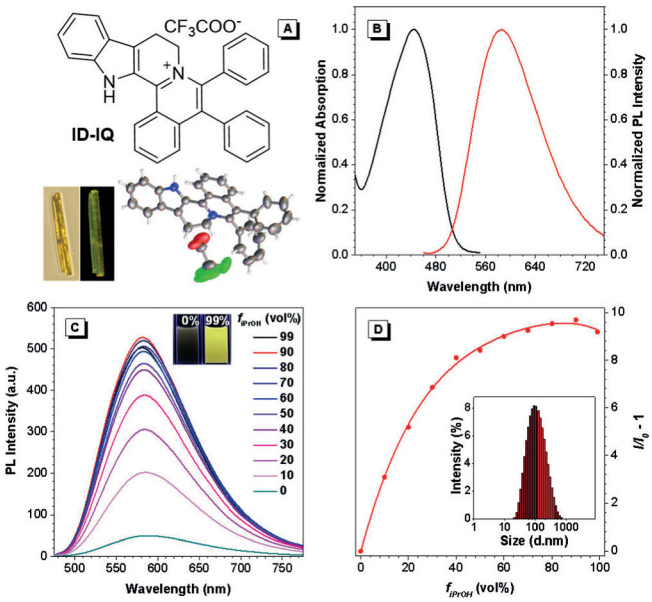

Figure 1. Structure and general properties of **ID-IQ**. A) Chemical and single crystal structure of **ID-IQ**. Inset: images of rod-shaped crystal of **ID-IQ** under ambient lighting and fluorescent microscope with blue light excitation (460–490 nm). B) Normalized absorption spectrum of **ID-IQ** (10 μM) in DMSO and emission spectrum in the solid state with 450 nm excitation. C) PL of **ID-IQ** (10 μM) in mixtures of THF and iPrOH with different iPrOH content (f_{iPrOH}). Inset: Fluorescence images of **ID-IQ** in THF solution and aggregated state (99% iPrOH) with 365 nm excitation. D) Plots of the relative emission intensity of **ID-IQ** versus iPrOH fraction. I_0 and I are the peak values of PL intensities of **ID-IQ** (10 μM) in THF and THF/iPrOH mixtures, respectively. Inset: size distribution of **ID-IQ** in the mixture of THF/ iPrOH with 99% iPrOH content.

a series of technical problems encountered in cytogenetic analysis such as the difficulties on overlapping chromosomes segmentation, centromeres identification, and specific genes mapping on chromosomes could be easily resolved. The compatibility of **ID-IQ** staining and FISH was also successfully demonstrated.

ID-IQ was synthesized through a $[RhCp^*Cl_2]_2$-catalyzed [4+2] annulation reaction in 86% yield and was characterized by ^{1}H-, ^{13}C-, and ^{19}F-NMR spectroscopy and high-resolution mass spectrometry (see the Supporting Information). The structure was further confirmed by x-ray single-crystal diffraction (Figure 1A and Table S1). The optical properties of **ID-IQ** were illustrated in Table S2. The maximum absorption peak at 449 nm (Figure 1B) and emission peak at 587 nm in DMSO solution with a large Stokes shift of 138 nm were observed. We then used mixed solvent (tetrahydrofuran/ isopropanol, THF/iPrOH) with different iPrOH fractions as the solvent system to evaluate the AIE. As depicted in Figure 1C and the Supporting Information, Figure S1, **ID-IQ** showed low fluorescence emission at 579 nm in THF solution. Adding iPrOH to the THF solution led to aggregate formation with gradual enhancement of the emission. The fluorescence intensity of **ID-IQ** in 99% iPrOH solution was 9.2-fold higher than that in pure THF (Figure 1D). The aggregate formation was confirmed by dynamic light scattering (DLS) analysis (Figure 1D and Figure S2). The emission enhancement could be explained by the restriction of rotational motion in the aggregated state. As shown in Figure S3, after adding glycerol to glycol solution, the viscosity increased, and the fluorescence intensity of **ID-IQ** showed a 2.3-fold increase with a blue-shift of the maximum emission from 584 nm to 563 nm. The quantum yields in the solid state (17.4%) and in the aggregation state (11.6%) were higher than that in solution (2.09%), indicating the typical AIE characteristic of **ID-IQ**.

Interestingly, when we tested the staining performance of **ID-IQ** on chromosome samples from human embryonic stem (hES2) cells, it showed that the chromosome boundary could be labelled by **ID-IQ**. As shown in Figure 2, after simply incubating the fixed chromosome with 10 μM **ID-IQ** and 20 μM Hoechst 33342 at 37 °C for 60 min, the fluorescence signal from **ID-IQ** (yellow) clearly highlighted the edge of the chromosome, which complemented the chromosome DNA stained by Hoechst 33342, demonstrating the high affinity of **ID-IQ** toward the CP structure.

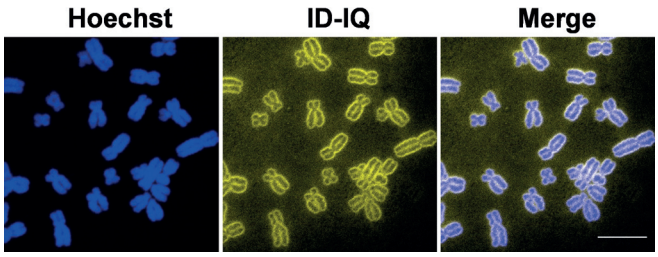

Figure 2. Fluorescence imaging of chromosomes (from hES2 cells) with Hoechst 33342 and **ID-IQ**. The chromosome body was labelled by Hoechst 33342 (blue). The boundary of the chromosome was labelled by **ID-IQ** (yellow). Merged image shows the overlay of two channels. Scale bar = 10 μm. (Hoechst 33342, λ_{ex} = 405 nm, λ_{em} = 430–480 nm; **ID-IQ**, λ_{ex} = 488 nm, λ_{em} = 530–630 nm).

It has been reported that proteins are the main component of the CP.[6] We suspected that the AIE-active probe **ID-IQ** interacted with these proteins and thus exhibited the enhanced signal on the CP structure. To verify this hypothesis, a digestion experiment was conducted. Proteinase K, a highly active serine protease with broad cleavage specificity on native and denatured proteins, was selected to digest the proteins on CP.[14] Fixed chromosomes from hES2 cells were treated with different concentrations of proteinase K ranging from 0.01 mM to 5 mM followed by staining with Hoechst 33342 and **ID-IQ** (Figure S5). The results showed that **ID-IQ** was able to label the boundary of chromosomes that were treated with low concentration of proteinase K. Increasing the concentration of proteinase K to 0.1 mM or above caused the loss of CP signal and the swelling of chromosomes, suggesting that the digestion of CPPs resulted in the loss of CP selectivity of **ID-IQ**. These results suggested that **ID-IQ** targeted the CP by binding to CPPs. Since DNA is another major component of the chromosome, we performed the experiment to investigate the relation between **ID-IQ** fluorescence and DNA content (Figure S6). The photoluminescence (PL) spectra showed that the fluorescence intensity of **ID-IQ** at the peak emission of 584 nm decreased with the

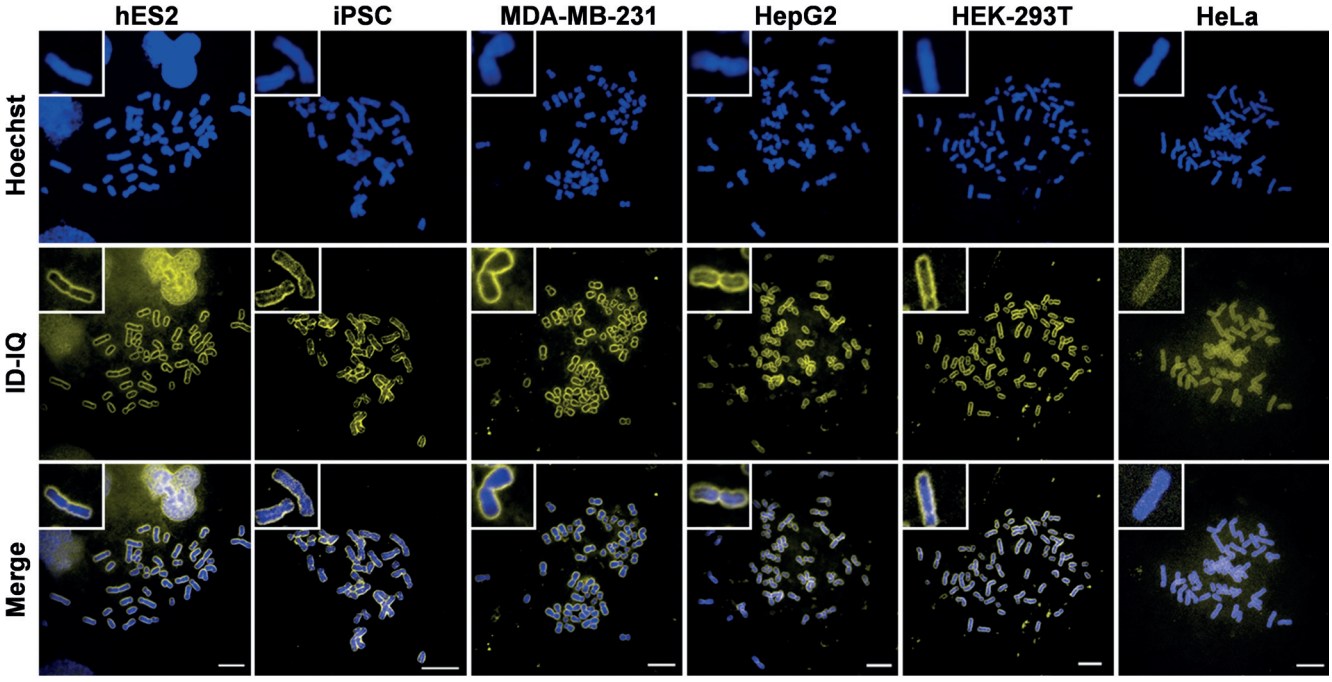

Figure 3. The CP of different cell types stained by **ID-IQ**. The DNA of the chromosome was labelled by Hoechst 33342. Scale bar = 10 μm. Inset: Enlarged images of corresponding panels.

addition of DNA. This implies that DNA would suppress the fluorescence signal of **ID-IQ** on the chromosome body, further enhancing the contrast of **ID-IQ** staining on the CP structure.

Subsequently, the feasibility of CP imaging in different cell types was investigated. As shown in Figure 3, **ID-IQ** demonstrated a highly specific labelling to the CP in stem cells (hES2 and induced pluripotent stem cells, iPSCs), cancer cells (breast cancer cells, MDA-MB-231 and hepatocellular carcinoma cells, HepG2) and normal cells (human embryonic kidney cells, HEK-293T). In all cell types examined, **ID-IQ** stained the CP. However, HeLa cells showed a faint chromosome boundary with **ID-IQ** staining, which may due to the altered protein components in this cancer cell type.[15]

These results prompted us to further explore the application of CP imaging with **ID-IQ** for cytogenetic studies. Chromosome segmentation is the first step for chromosome analysis.[16] It is of great interest to develop a method to assist the chromosome analysis in chromosome recognition, identification, and separation, especially when there are chromosome clusters. Although computational analysis has currently been used for segregation of overlapping or touching chromosomes, the accuracy of the post-analysis still largely depends on the original chromosome images. Therefore, it is preferred to directly obtain clear chromosome images.[17] By highlighting the CP, the chromosome surface structure, **ID-IQ** demonstrated a great advantage in assisting the segmentation of chromosome images. As shown in Figure 4 A–C, it was hard to segment the overlapping chromosomes in the cluster by the Hoechst 33342 signal (Figure 4 A). On the other hand, the boundary of the chromosomes could be easily identified with the help of **ID-IQ** (Figure 4 B,C), which would aid the cytogeneticist to distinguish the upper short chromosome

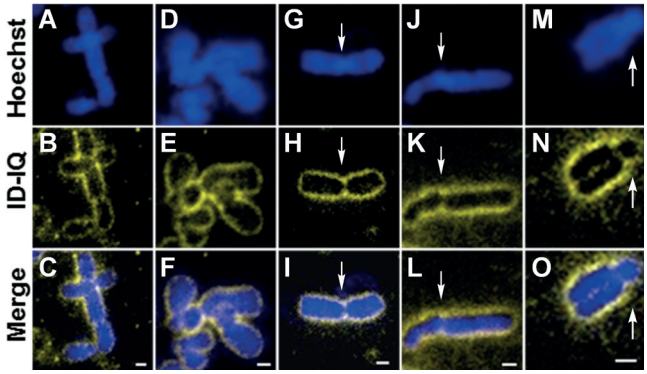

Figure 4. CP labelling by **ID-IQ**-assisted chromosome analysis. A–C) **ID-IQ** highlighted the edge of chromosomes, which provided essential information to separate the overlapped chromosomes. D–F) **ID-IQ** labelled the edge of the chromosomes, which helped separating the adjacent chromosomes. G–O) Arrows indicate the centromere's position. **ID-IQ** could be used for differentiating different types of chromosomes, including metacentric (G–I), submetacentric (J–L), and acrocentric (M–O) chromosomes. Scale bar = 1 μm.

from the lower longer one. In addition, even the cluster of touching chromosomes could be easily segmented with the help of **ID-IQ** (Figure 4 D–F).

Chromosome morphology identification is another important task in chromosome analysis. Classification of chromosome morphology is based on the position of the centromere, the most constricted region of the chromosome. Precisely locating the centromere position is thus crucial for the correct measurement of the chromosomal arm length, classification of the chromosome type, and description of the position of genes on chromosomes. Visualizing the centromere could be

affected by the low quality of the image resolution or shape of chromosomes (Figure 4G,J,M). Difficulty in locating the centromere position has often been encountered by cytogeneticists. Morphologically, the chromosomes boundary labelled with **ID-IQ** would curve inward in the position of centromere, which indicates the position of the centromere (Figure 4H,K,N). Therefore, it is easy to identify different chromosomes types based on **ID-IQ** staining. Figure 4G–O displays chromosomes in various types. With the centromere positioned, we could intuitively identify chromosomes of different morphology, for example, submetacentric (Figure 4G–I), metacentric (Figure 4J–L), and acrocentric (Figure 4M–O). In addition, the chromosomal arm length, which was also essential information for chromosome analysis, could be measured easily as well after the chromosome had been sharply outlined. **ID-IQ** provided us a rapid and promising approach to assist the chromosome studies, which illustrated a great potential in its further application in combination with other cytogenetic techniques that are based on fluorescence.

Due to the complicated physiological environment, stringent sample preprocessing procedures are inevitable when performing clinical diagnosis. To demonstrate its practical application in clinical cytogenetics, we further tested the compatibility of **ID-IQ** staining with FISH. Herein, human lymphocyte chromosomes were prepared and co-stained with **ID-IQ** and a FISH centromere probe. As mentioned, **ID-IQ** had an inherent advantage for assisting the identification of the centromere position. A co-localization experiment was performed with a FISH probe targeting the centromere. As shown in Figure 5A–G and Figure S7, the position of the centromere, highlighted by the FISH probe (red), could hardly be identified by the DAPI signal (blue) but could be clearly visualized in the **ID-IQ** channel (yellow). It is worth mentioning that the FISH probe displayed a relatively larger spot (Figure 5C) while **ID-IQ** could indicate the precise position of centromere on chromosomes with a better spatial resolution (Figure 5E).

To further demonstrate that the co-staining by **ID-IQ** with FISH could help researchers to locate a particular gene on the chromosome, we co-stained the chromosome with **ID-IQ** and other FISH probes. In this study, we used a chromosome 4q telomere FISH probe, which targeted the long arm telomere on chromosome 4. The telomere is an important component for chromosomes, which is directly associated with cell apoptosis.[8c] The existence of telomere is necessary in protecting chromosomes from chemical modification or nucleic acid degradation. As shown in Figure 5H–N and Figure S8, limited information on the FISH probe position could be obtained from the overlaid image with the chromosome body counterstained by DAPI (blue, Figure 5I,K), not even to distinguish if it was on the short or long arm of the chromosome. Without highlighting the location of the centromere and chromosome boundary, it would be difficult to tell if there is any chromosomal abnormality in the absence of its relative position on chromosomes. The **ID-IQ** signal (yellow, Figure 5L,N) clearly showed the location of the centromere and outlined both long arms and short arms, which allowed us to locate the relative position of the interested gene. As shown in Figure 5M, this FISH probe

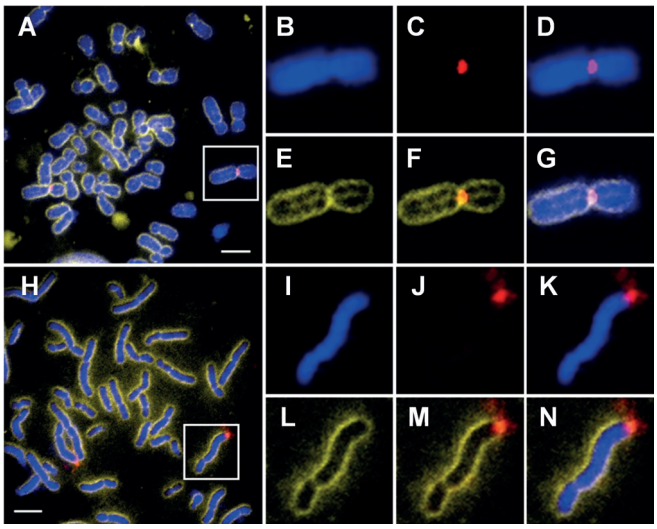

Figure 5. Lymphocyte chromosomes co-stained by **ID-IQ** (yellow), DAPI (blue) and A) centromere-specific FISH probe (red) or (H) chromosome 4q telomere FISH probe (red). The corresponding enlarged views of selected chromosomes (highlighted in white box) in different channels and merged images are given in (B–G) or (I–N), respectively. B) The chromosomal body labelled by DAPI and C) the centromere labelled by FISH probe. D) Merged image of (B) and (C). E) The CP and the centromere were highlighted by **ID-IQ**. F) Merged image of (C) and (E). G) Merged image of the three channels. I) The chromosomal body labelled by DAPI and J) the telomere labelled by chromosome 4q telomere probe. K) Merged image of (I) and (J). L) The CP and the centromere were highlighted by **ID-IQ**. M) Merged image of (J) and (L), indicating that the 4q telomere FISH probe located in the long arm of this chromosome. N) Merged image of all three channels. Scale bar = 5 μm.

labelled the telomere at the end of the long arm of chromosomes. **ID-IQ** staining was also used to locate the FISH telomere probe in X and Y chromosomes, which further confirmed its compatibility with FISH technique (Figure S9). Together, technical challenges in chromosome analysis such as centromere identification or chromosome classification could be solved by inherent advantages of **ID-IQ** staining, indicating its great potential in clinical research and diagnosis.

In summary, we reported the first small-molecule fluorescent probe, **ID-IQ,** for CP imaging. **ID-IQ** showed AIE property with a large Stokes shift. **ID-IQ** allowed imaging the CP in different cell types including stem cells, cancer cells, and normal cells. **ID-IQ** staining could light up the sharp chromosome boundary, which greatly facilitated the segmentation of chromosome clusters with overlapping or touching chromosomes. Furthermore, the centromere position of **ID-IQ** stained chromosomes could be clearly identified, which allowed researchers to easily distinguish chromosomes in different morphologies and to accurately estimate the chromosomal arm length. In combination with the FISH technique, researchers could locate a gene on the chromosome with high accuracy. **ID-IQ** provided a rapid and reliable approach to assist the chromosome studies, and we envision its great potential for application in clinical cytogenetics and quality control in cell therapy manufacturing.

Acknowledgements

We thank Yuk-Fong Tang from Queen Mary Hospital for assistance with lymphocyte chromosomes preparation and FISH labelling, Tian Jiang and Dr. Thomas Balle from the University of Sydney for their help in data analysis, Dr. Engui Zhao for proofreading our manuscript. S.C. acknowledges the start-up funding from Ming Wai Lau Centre for Reparative Medicine, Karolinska Institutet. M.-Y.W. is grateful to financial support from the National Natural Science Foundation of China (21708030).

Conflict of interest

The authors declare no conflict of interest.

Keywords: aggregation-induced emission · centromeres · chromosome analysis · chromosome periphery · fluorescence imaging

[1] P. Benn, *J. Clin. Med.* **2014**, *3*, 1291 – 1301.
[2] a) P. Catalina, F. Cobo, J. L. Cortes, A. I. Nieto, C. Cabrera, R. Montes, A. Concha, P. Menendez, *Cell Biol. Int.* **2007**, *31*, 861 – 869; b) The International Stem Cell Banking Initiative, *Stem Cell Rev.* **2009**, *5*, 301 – 314.
[3] a) M. Manning, L. Hudgins, Professional Practice and Guidelines Committee, *Genet. Med.* **2010**, *12*, 742 – 745; b) D. Moralli, M. Yusuf, M. A. Mandegar, S. Khoja, Z. L. Monaco, E. V. Volpi, *Stem Cell Rev. Rep.* **2011**, *7*, 471 – 477.
[4] a) M. V. Munot, J. Mukherjee, M. Joshi, *Med. Biol. Eng. Comput.* **2013**, *51*, 1325 – 1338; b) P. R. Langer-Safer, M. Levine, D. C. Ward, *Proc. Natl. Acad. Sci. USA* **1982**, *79*, 4381 – 4385.
[5] a) E. Strasburger, *Arch. Mikrosk. Anat.* **1882**, *21*, 476 – 588; b) D. G. Booth, A. J. Beckett, O. Molina, I. Samejima, H. Masumoto, N. Kouprina, V. Larionov, I. A. Prior, W. C. Earnshaw, *Mol. Cell* **2016**, *64*, 790 – 802; c) D. G. Booth, M. Takagi, L. Sanchez-Pulido, E. Petfalski, G. Vargiu, K. Samejima, N. Imamoto, C. P. Ponting, D. Tollervey, W. C. Earnshaw, P. Vagnarelli, *eLife* **2014**, *3*, e01641.
[6] D. G. Booth, W. C. Earnshaw, *Trends Cell Biol.* **2017**, *27*, 906 – 916.
[7] a) C. W. Metz, *Proc. Natl. Acad. Sci. USA* **1934**, *20*, 159 – 163; b) S. Matsunaga, K. Fukui, *Biomol. Concepts* **2010**, *1*, 157 – 164.
[8] a) T. Hirano, R. Kobayashi, M. Hirano, *Cell* **1997**, *89*, 511 – 521; b) R. Poonperm, H. Takata, T. Hamano, A. Matsuda, S. Uchiyama, Y. Hiraoka, K. Fukui, *Sci. Rep.* **2015**, *5*, 11916; c) R. J. O'Sullivan, J. Karlseder, *Nat. Rev. Mol. Cell Biol.* **2010**, *11*, 171 – 181; d) A. F. Pluta, A. M. Mackay, A. M. Ainsztein, I. G. Goldbeg, W. C. Earnshaw, *Science* **1995**, *270*, 1591 – 1594; e) F. G. Westhorpe, A. F. Straight, *Curr. Opin. Cell Biol.* **2013**, *25*, 334 – 340.
[9] a) A. A. Van Hooser, P. Yuh, R. Heald, *Chromosoma* **2005**, *114*, 377 – 388; b) S. Uchiyama, S. Kobayashi, H. Takata, T. Ishihara, N. Hori, T. Higashi, K. Hayashihara, T. Sone, D. Higo, T. Nirasawa, T. Takao, S. Matsunaga, K. Fukui, *J. Biol. Chem.* **2005**, *280*, 16994 – 17004.
[10] a) M. Grossi, M. Morgunova, S. Cheung, D. Scholz, E. Conroy, M. Terrile, A. Panarella, J. Simpson, W. M. Gallagher, D. F. O'Shea, *Nat. Commun.* **2016**, *7*, 10855; b) X. Zheng, X. Wang, H. Mao, W. Wu, B. Liu, X. Jiang, *Nat. Commun.* **2015**, *6*, 5834.
[11] J. Luo, Z. Xie, J. W. Y. Lam, L. Cheng, H. Chen, C. Qiu, H. S. Kwok, X. Zhan, Y. Liu, D. Zhu, B. Z. Tang, *Chem. Commun.* **2001**, 1740 – 1741.
[12] a) J. Mei, N. C. Leung, R. T. K. Kwok, J. W. Y. Lam, B. Z. Tang, *Chem. Rev.* **2015**, *115*, 11718 – 11940; b) R. T. K. Kwok, C. W. T. Leung, J. W. Y. Lam, B. Z. Tang, *Chem. Soc. Rev.* **2015**, *44*, 4228 – 4238; c) Y. Hong, J. W. Y. Lam, B. Z. Tang, *Chem. Soc. Rev.* **2011**, *40*, 5361 – 5388; d) Z. Guo, C. Yan, W. H. Zhu, *Angew. Chem. Int. Ed.* **2019**, https://doi.org/10.1002/anie.201913249; *Angew. Chem.* **2019**, https://doi.org/10.1002/ange.201913249.
[13] a) J. Qian, B. Z. Tang, *Chem* **2017**, *3*, 56 – 91; b) S. Xie, A. Y. H. Wong, S. Chen, B. Z. Tang, *Chem. Eur. J.* **2019**, *25*, 5824 – 5847; c) C. Zhu, R. T. K. Kwok, J. W. Y. Lam, B. Z. Tang, *ACS Appl. Bio Mater.* **2018**, *1*, 1768 – 1786.
[14] H. Hilz, U. Wiegers, P. Adamietz, *Eur. J. Biochem.* **1975**, *56*, 103 – 108.
[15] a) M. Dobles, V. Libera, M. L. Scott, R. Benezra, P. K. Sorger, *Cell* **2000**, *101*, 635 – 645; b) M. Dobles, P. K. Sorger, *Cold Spring Harbor Symp. Quant. Biol.* **2000**, *65*, 361 – 368; c) A. Gupta, S. Inaba, O. K. Wong, G. Fang, J. Liu, *Oncogene* **2003**, *22*, 7593 – 7599.
[16] S. Minaee, M. Fotouhi, B. H. Khalaj, *IEEE Signal Processing in Medicine and Biology Symposium*, **2014**.
[17] D. Somasundaram, V. R. Vijay Kumar, *Measurement* **2014**, *48*, 274 – 281.

Manuscript received: December 30, 2019
Revised manuscript received: February 4, 2020
Accepted manuscript online: March 12, 2020
Version of record online: April 6, 2020

